Drift Orbits and Drift-Orbit Pumping in Thermal Barriers

D.G. Braun and G.A. Emmert

February 1981

UWFDM-403

Presented at the 22nd Annual Meeting of the Division of Plasma Physics, APS, Nov. 10-14, 1980, San Diego, CA.

FUSION TECHNOLOGY INSTITUTE

UNIVERSITY OF WISCONSIN

MADISON WISCONSIN

Drift Orbits and Drift-Orbit Pumping in Thermal Barriers

D.G. Braun and G.A. Emmert

Fusion Technology Institute
University of Wisconsin
1500 Engineering Drive
Madison, WI 53706

http://fti.neep.wisc.edu

February 1981

UWFDM-403

Presented at the 22nd Annual Meeting of the Division of Plasma Physics, APS, Nov. 10-14, 1980, San Diego, CA.

Drift Orbits and Drift-Orbit Pumping in Thermal Barriers

D. G. Braun and G. A. Emmert

Fusion Engineering Program
Nuclear Engineering Department
University of Wisconsin
Madison, WI 53706

February 1981

UWFDM-403

Presented at the 22nd Annual Meeting of the Division of Plasma Physics, American Physical Society, 10-14 Nov., 1980, San Diego

Abstract

The effectiveness of drift-orbit pumping of thermal barriers is analyzed by calculating constant J surfaces of barrier trapped ions. The calculations are for two magnetic configurations: a double yin-yang, which produces an elliptical barrier, and an inboard barrier which is circular at one end and elliptical at the other end. In both cases, drift-orbit pumping is relatively ineffective. This is because the radial electric field produces an $\vec{E} \times \vec{B}$ drift which limits the excursion of trapped ions from the flux surfaces.

I. Introduction

A significant improvement in tandem mirror confinement is made by creating a thermal barrier between the end plug and central cell sections.[1] The thermal barrier is a region of reduced magnetic field strength and plasma density; this creates a dip in the electrostatic potential and thermally insulates the plug electrons from the central cell electrons. The plug electrons can then be heated to, and maintained at a higher temperature than the electrons in the central cell. Consequently, for a fixed plug-central cell density ratio, a larger plug potential is obtained, and hence there is better central cell confinement.

Collisional scattering will, however, cause ions to become trapped in the electrostatic well formed by the barrier. This reduces the density depression and the barrier potential dip. Sustaining the barrier requires that these trapped particles in the barrier be removed (i.e. "pumped out"). This pumping mechanism could be accomplished by neutral beam injection at low pitch angle which, via charge exchange, converts the trapped particles back into the streaming component. Another method of barrier pumping is the use of RF power to heat the parallel motion of the ions and hence detrap them. Both of these methods represent an increase in input power.[2] Kesner[3] noted that the drift motion of particles trapped in the barrier cell could deviate significantly from the flux surfaces by grad-B drift effects if the flux tube is elliptical there. Streaming particles from the central cell, which one would not want to remove, would stay on the flux surfaces, but trapped plasma would drift away from the surfaces where it could be collected on a limiter. This method of passive pumping would thus require no energy input in the barrier, but it does represent an energy drain from the central cell.

Baldwin[4] has noted some problems with this passive pumping scheme, foremost of which is the removal of barrier trapped electrons that are also pumped. These electrons may be desired in order to enhance the barrier potential dip. He further points out that the radial electric field will produce an azimuthal $\vec{E} \times \vec{B}$ drift that will follow nearly the flux surfaces. This drift will compete with the grad-B drift and will limit the effectiveness of drift-orbit pumping.

In this paper, the drift surfaces of these barrier trapped particles will be calculated to determine the extent of this passive pumping. It will be assumed that the bounce frequency of the trapped particles is much greater than their collision frequency. Hence, the particle dynamics will be assumed to be collisionless, with parallel motion described by guiding center theory. The magnetic moment, μ, is then a constant of the motion, along with the total particle energy E, and the second adiabatic invariant

$$J = \oint v_{\parallel} \, ds \quad .$$

Since J is conserved, the trapped particles' drift surfaces will be the surfaces of constant J.

The parallel velocity is a function of the local magnetic field and the local electrostatic potential,

$$v_{\parallel}(s) = \left(\frac{2}{m} [E - \mu B(s) - e\phi(s)]\right)^{1/2} \quad . \tag{1}$$

Drift surfaces are calculated at the barrier minimum, where particles are launched with initial velocity components $v_{\perp}$ and $v_{\parallel}$, relative to the magnetic

field direction. These, together with the values of the magnetic field and electrostatic potential at the point of launching, determine the constants E and μ. With these constants Eq. (1) can be used to determine the parallel velocity of a particle along various field lines in the barrier, and values of J can be calculated numerically.

The value of B(s) along the field lines used is calculated by the EFFI code, but the value of $\phi(s)$ along these lines must also be calculated. Section II of this report describes how the electrostatic potential is determined along a particular field line. Section III gives the results of this drift surface analysis for a coil configuration where drift-orbit pumping should be strong. In Section IV the WITAMIR-I tandem mirror reactor design[2] is analyzed for the effect of this pumping.

II. The Electrostatic Potential Model

The model used to determine the electrostatic potential throughout the barrier cell calculates the potential relative to an assumed $\phi = 0$ in the central cell, on axis. The potential change from this value is achieved in two steps. First, a radial potential drop, $\Delta\phi_r$, is assumed in the central cell in going from the axis to a particular field line. In this calculation a Gaussian model is used, with a defined plasma radius R, to determine the potential drop; that is,

$$\Delta\phi_r = \phi_{cc}(1 - e^{(r/R)^2}) \qquad (2)$$

where ϕ_{cc} is the potential of the central cell (on axis) relative to ground. The actual radial potential profile is determined by the transport processes in the central cell and end plug. Equation (2) is chosen for simplicity; its

only justification is that it resembles the results of tandem mirror transport simulation codes.[5] The second step in determining the barrier potential is then the variation along the field line, $\Delta\phi_{FL}$, which is a function of the magnetic field through the barrier. The evaluation of this second potential variation will now be described in more detail.

The equations that determine this potential change along a field line start with an analysis of velocity space to determine the extent of plug electrons vs. central cell electrons. In Fig. 1 the typical variation of magnetic field and potential along a field line is shown schematically through a thermal barrier and end plug. Two zones are used for the analysis of the electron density. In the first zone, between points A and B, the electrons are assumed to belong to the central cell population, which is assumed to be Maxwellian at temperature T_{ec}. However, in the second zone, between points B and C, there will be a mixing of central cell and plug electrons, which are at different temperatures.

For the plug side of the barrier, the equations of conservation of E and μ for electrons relative to point B,

$$\frac{1}{2} mv_{\parallel}^2 + \frac{1}{2} mv_{\perp}^2 - e\phi = \frac{1}{2} mv_{\parallel}^2\Big|_B + \frac{1}{2} mv_{\perp}^2\Big|_B - e\phi_B \tag{3}$$

$$\frac{1}{2} mv_{\perp}^2 \,/\, B = \frac{1}{2} mv_{\perp}^2 \,/\, B\Big|_B \tag{4}$$

yield

$$\frac{1}{2} mv_{\parallel}^2(s) + \frac{1}{2} mv_{\perp}^2(s)\left(1 - \frac{B\big|_B}{B(s)}\right) = e(\phi(s) - \phi_B) + \frac{1}{2} mv_{\parallel}^2\Big|_B \quad . \tag{5}$$

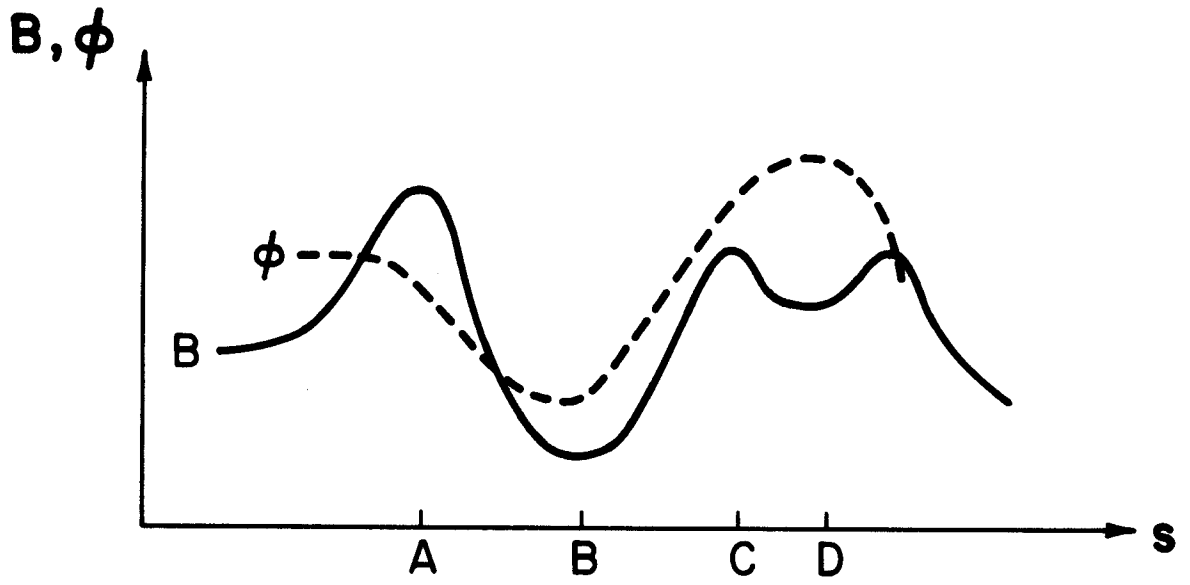

Figure 1. Typical magnetic field and electrostatic potential variation through a thermal barrier and end plug.

Equation (5) defines an ellipse in velocity space, shown in Fig. 2, at each point along a field line characterized by B(s). Those electrons outside the ellipse have $v_{\parallel}\Big|_B > 0$, i.e. they can pass over the potential barrier. These electrons spend most of their time mixing with central cell electrons, and hence are considered central cell electrons. Those inside the ellipse are reflected by the potential barrier and are assumed to be the hotter plug electrons. At s = B the ellipse has zero size and all the electrons are then considered central cell electrons, as one would expect.

For the ion dynamics one only considers those ions streaming from the central cell through the barrier into the plug. As a first approximation, we assume drift-orbit pumping is effective, and therefore ignore trapped ions in the thermal barrier. Calculating the potential variation along a field line relative to $\phi = 0$ in the central cell, two cases appear: $\phi(s) < 0$ and $\phi(s) > 0$. The former has already been treated by Kesner.[6] When $\phi(s) > 0$, there is a reflection of some of the streaming ions off the plug potential peak. Equations of conservation of E and μ, similar to Eqs. (3) and (4) only for ions, yield

$$\frac{1}{2} mv_{\parallel}^2(s) + \frac{1}{2} mv_{\perp}^2(s) \left(1 - \frac{B\Big|_A}{B(s)}\right) = -e\phi(s) + \frac{1}{2} mv_{\parallel}^2\Big|_A \qquad (6)$$

where point A has been taken as the reference and it is assumed $\phi\Big|_A = 0$. Equation (6) divides velocity space as shown in Fig. 3. The shaded area between the hyperboli is the streaming ions for which $v_{\parallel}^2\Big|_A > 0$.

We now assume that, in the populated regions of velocity space, the distribution functions are Maxwellian, with temperature T_{ec} for central cell electrons, T_{ep} for plug electrons and T_i for the streaming ions. Integration

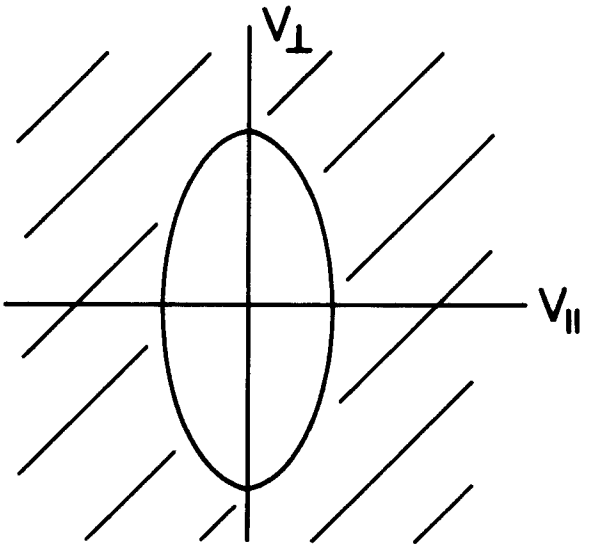

Figure 2. Velocity space for electrons between points B and C. Shaded region represents electrons that pass over the barrier potential, ϕ_b, and enter the central cell.

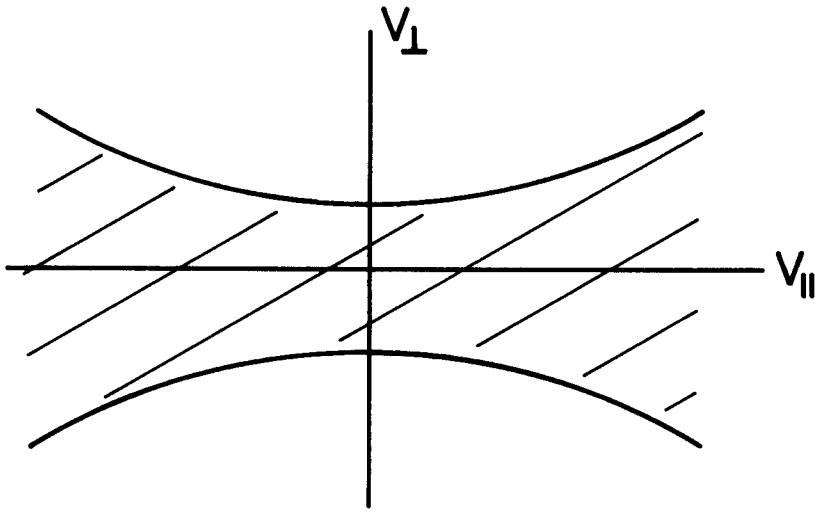

Figure 3. Velocity space for ions between points B and D. Shaded region represents streaming ions.

over velocity space and quasi-neutrality yield the following equations which can be solved for $\phi(s)$:

for $A \leq s \leq B$

$$e^{e\phi/T_{ec}} = e^{-e\phi/T_i} \operatorname{erfc}\sqrt{\frac{e\phi}{T_i}} - \frac{1}{\sqrt{\gamma}} e^{-\gamma e\phi/T_i} \operatorname{erfc}\sqrt{-\frac{e\gamma\phi}{T_i}} \quad ; \qquad (7)$$

for $B \leq s$, $\phi < 0$

$$e^{e\phi/T_{ec}} [1 - F(\phi,T_{ec})] + \frac{A_p}{n_c} e^{e\phi/T_{ep}} F(\phi,T_{ep})$$

$$= e^{-e\phi/T_i} \operatorname{erfc}\sqrt{-\frac{e\phi}{T_i}} - \frac{1}{\sqrt{\gamma}} e^{-\gamma e\phi/T_i} \operatorname{erfc}\sqrt{-\frac{\gamma e\phi}{T_i}} \quad ;$$

for $B \leq s$, $\phi > 0$

$$e^{e\phi/T_{ec}} [1 - F(\phi,T_{ec})] + \frac{A_p}{n_c} e^{e\phi/T_{ep}} F(\phi,T_{ep}) = e^{-e\phi/T_i} - \frac{1}{\sqrt{\gamma}} e^{-\gamma e\phi/T_i}$$

where

$$F(\phi,T) = \operatorname{erf}\sqrt{\frac{e(\phi - \phi_B)}{T}} - \frac{2}{\sqrt{\pi\delta}} e^{-(\delta+1)e(\phi-\phi_B)/T} D\left(\sqrt{\frac{\delta e(\phi - \phi_B)}{T}}\right)$$

$$\gamma = \frac{1}{1 - \frac{B}{B|_A}} \qquad \delta = \frac{1}{\frac{B}{B|_B} - 1}$$

$$D(x) = \int_0^x e^{t^2} dt \qquad A_p = n_D e^{-e\phi_D/T_{ep}} \quad .$$

The input to Eqs. (7) are the plug and central cell densities, n_c and n_D, the

plug-central cell potential difference ϕ_D, and the temperatures T_{ec}, T_{ep} and T_i. The radial dependence of temperature and density is included by using a Gaussian, similar to that for $\Delta\phi_r$, for n_c, T_{ec} and T_i.

Equations (7) give the potential variation along a field line, but have two deficiencies. First, the potential drop at the barrier maximum, $\Delta\phi_{FL}\big|_A$, should be zero, but is calculated to be non-zero. Secondly, there is a multi-valuedness of $\Delta\phi_{FL}(s)$ around the transition region of $\Delta\phi_{FL} = 0$ on the plug side of the barrier. Li[7] has resolved both these discrepancies, the first by remodeling the ion distribution function and the second by the inclusion of electrons trapped by the barrier potential minimum and the plug magnetic field peak. In this calculation the multi-valuedness was removed by a linear approximation across the multiple-valued region.

Combining the radial drop of potential and the potential variation along a field line, $\Delta\phi_r$ and $\Delta\phi_{FL}$ gives the net potential throughout the barrier relative to $\phi = 0$ on axis in the central cell. Figure 4 illustrates the net potential variation along various field lines that intersect the y-axis at the barrier minimum for the coil configuration used in Section III of this report. The field line (0,14) (not shown) maps into r = R in the central cell. The radial potential drop in the central cell, and the effect of radial temperature variation which reduces the variation in $\Delta\phi_{FL}$ is evident. The wall potential is at -277 keV.

III. Drift-Orbit Pumping in a Double Yin-Yang Configuration

Drift-orbit pumping should be effective in a configuration like the so-called Double Yin-Yang, where one set of yin-yang coils serves as the magnetic barrier peak, and the other as the end plug, with a low B barrier cell between them. The coil arrangement is shown in Fig. 5. The flux tube through the

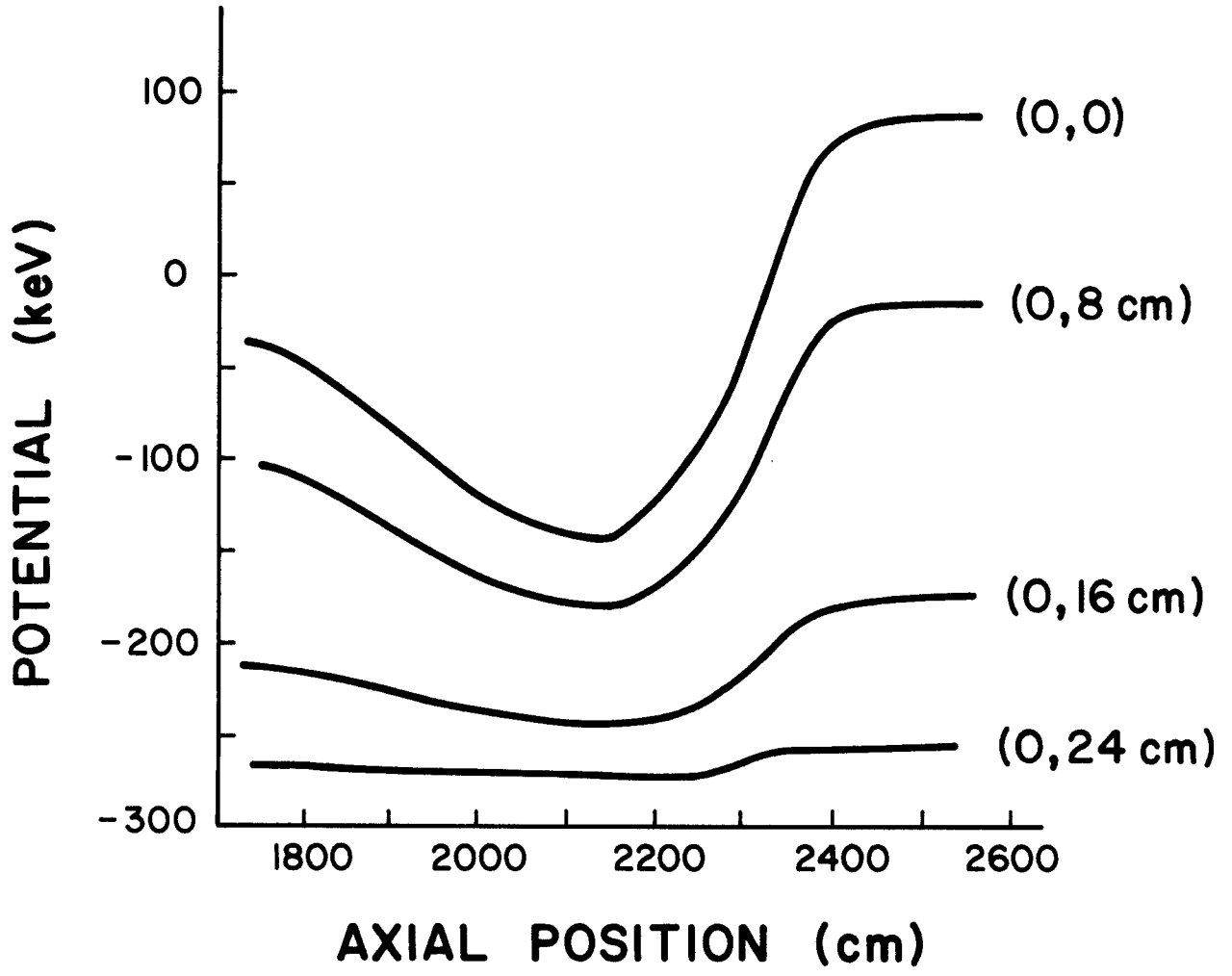

Figure 4. Axial variation of electrostatic potential along various field lines, double yin-yang configuration. The coordinates (x,y) are the coordinates of the field line where it intersects the barrier minimum.

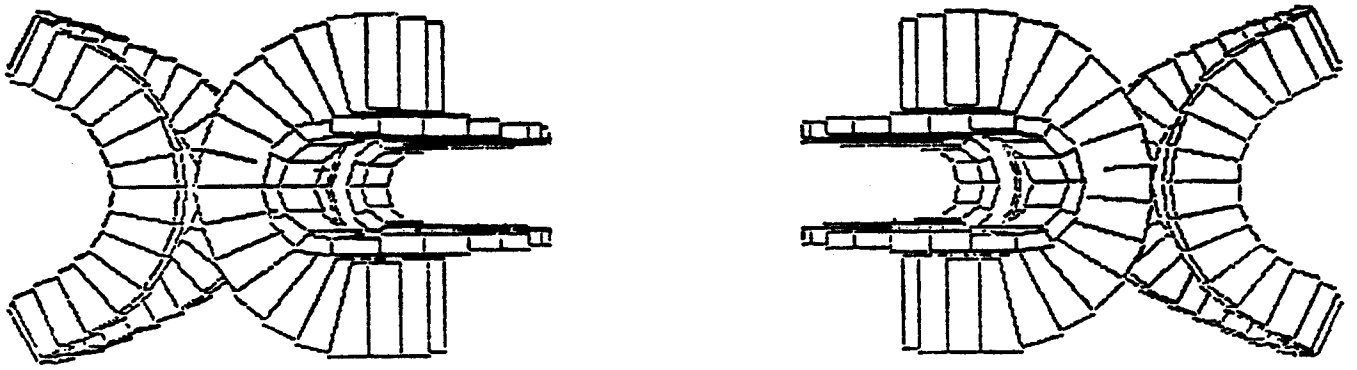

Figure 5. BARRIER COIL SET, DOUBLE YIN-YANG CONFIGURATION

barrier goes from circle to ellipse and back to circle. This is shown in Fig. 6 along with the axial magnetic field and potential calculated from Eqs. (7). The flux surfaces were obtained by tracing circular surfaces from the central cell through the barrier using the EFFI code. The plasma radius is assumed to be 100 cm in the central cell. This maps into an ellipse at the barrier magnetic field minimum with an ellipticity of 26.2. Because of this extreme elongation, one expects the trapped particles to have drift orbits which deviate considerably from the flux surfaces there. The barrier mirror ratio in this configuration is approximately 8.6 on axis.

The surfaces of constant potential deviate from the flux surfaces in this configuration. Equations (7) predict that the potential drop along a field line is primarily a function of the local barrier mirror ratio. Field lines on the same flux surface and having the same potential in the central cell will, in the non-axisymmetric barrier, have a different barrier mirror ratio and hence a different potential drop in each plane defined by a constant azimuthal angle, θ. For example, the 100 cm central cell flux tube has a maximum mirror ratio of 8.64 in the plane of the ellipse's minor axis. But along its major axis, which has a factor of 2 lower minimum B in the fan of the ellipse, the maximum mirror ratio is 15.9. The variation of potential across flux surfaces is illustrated in Fig. 7. The variation in the R = 100 cm flux surface is significant, 10.1 keV in an average potential drop of 57 keV. The variation of potential will affect the degree of thermal isolation provided by the barrier and create azimuthal electron temperature gradients in flux surfaces in the central cell. If these gradients are not removed by drifting central cell particles, they could give rise to azimuthal variations in the central

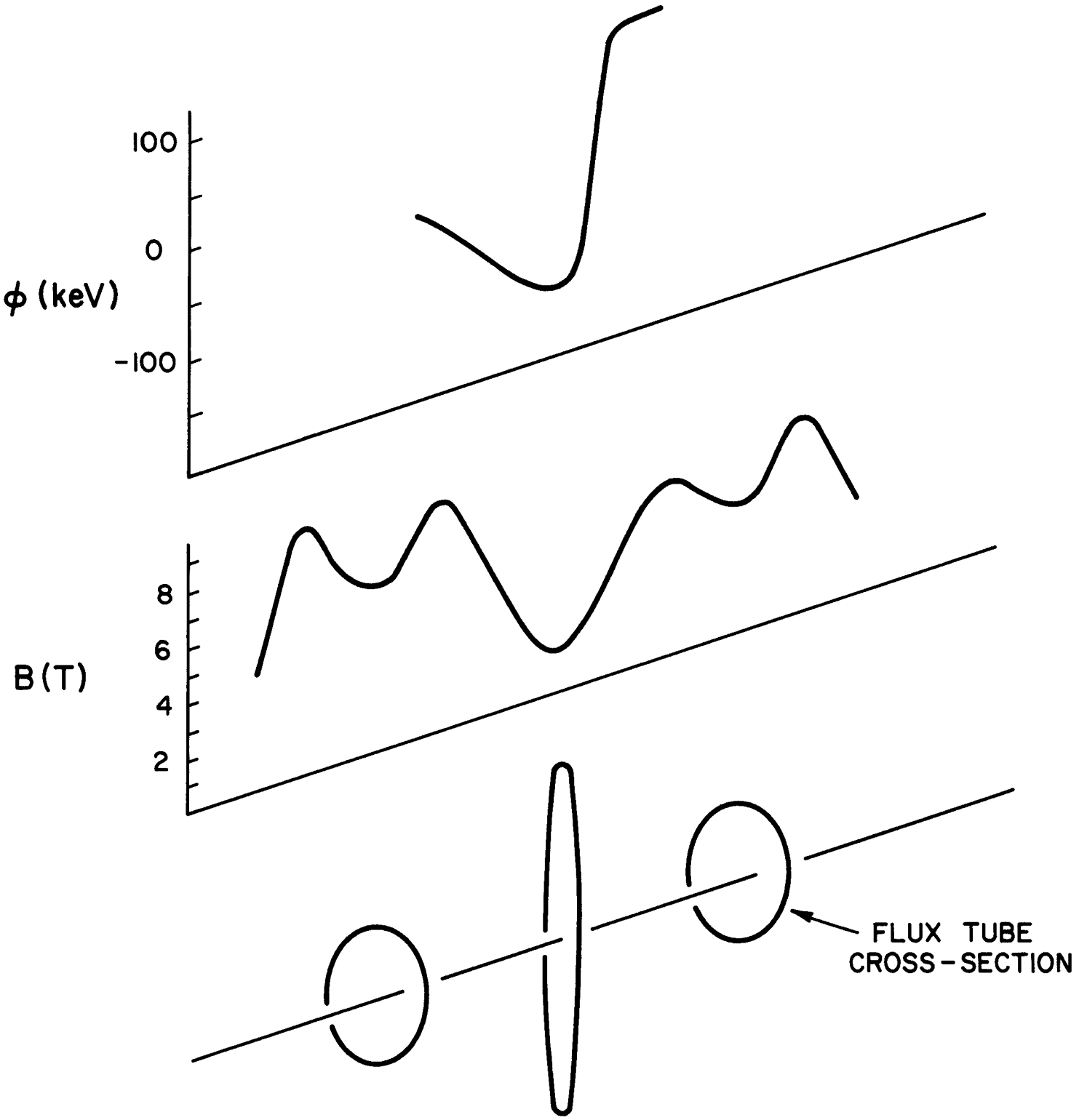

Figure 6. Flux tube cross-sections, at various axial locations in the barrier cell, and the on-axis magnetic field and potential for the double yin-yang configuration.

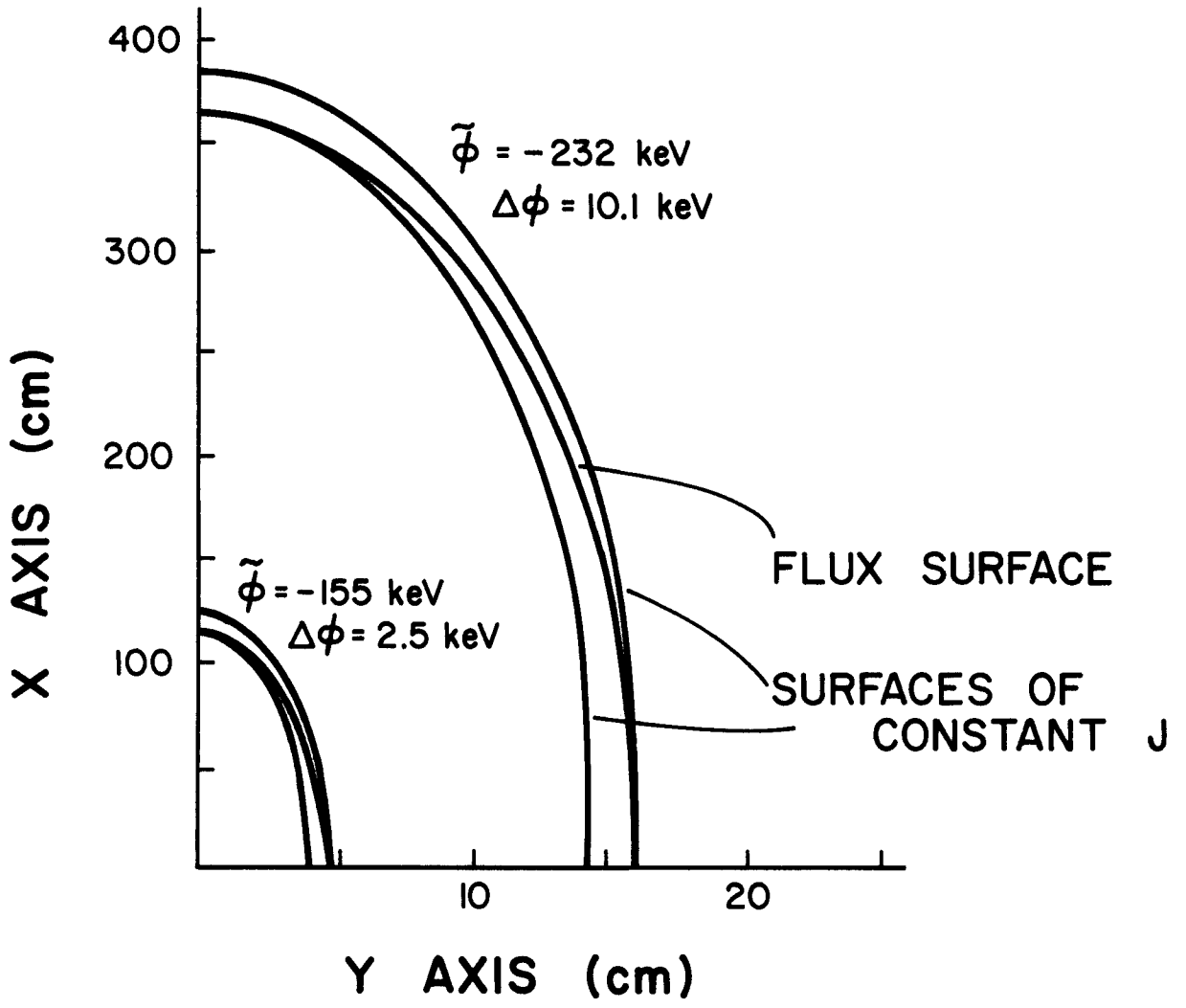

Figure 7. Variation of the potential in flux surfaces at the barrier minimum, double yin-yang configuration.

cell potential and hence cause enhanced plasma convection through the radial component of the $\vec{E} \times \vec{B}$ drift velocity.

The barrier trapped ions will have two competing azimuthal drifts, the $\vec{E} \times \vec{B}$ drift and the grad-B drift. These are compared in Fig. 8. The $\vec{E} \times \vec{B}$ drift will follow surfaces of constant ϕ, which are nearly the flux surfaces. Figure 8 clearly shows that if the drift surfaces, i.e. surfaces of constant J, follow a path similar to that of the grad-B rather than $\vec{E} \times \vec{B}$ drift, a large portion of the elliptical flux tube can be pumped. If the $\vec{E} \times \vec{B}$ drift dominates, however, then drift-orbit pumping is ineffective.

A sweep of velocity space was made at the barrier minimum for various points along the major axis of the ellipse. Particles were started with assigned velocities $v_\perp$ and $v_\parallel$ relative to the magnetic field there. These determine the constant E and μ for the particles. The value of J obtained is compared to the value of J calculated using the same E and μ at the plasma boundary at the minor axis to determine whether the particle would drift outside the plasma. The plasma input parameters used in this calculation are in Table 1.

The growth of the drift-orbit pumped region of velocity space as one moves up the major axis of the ellipse is shown in Fig. 9. Region I is the pumped region, II is the non-pumped, and Region III is the loss cone. The units are $keV^{1/2}$. The plasma's defined boundary at the barrier minimum is 367 cm along the major axis. Figure 9 shows that drift-orbit pumping starts to occur at 225 cm, roughly 2/3 of the way up the ellipse, and it shows that a large proportion of velocity space isn't pumped until 275-300 cm. This means that only the top 1/4 of the trapped plasma ellipse is being effectively pumped.

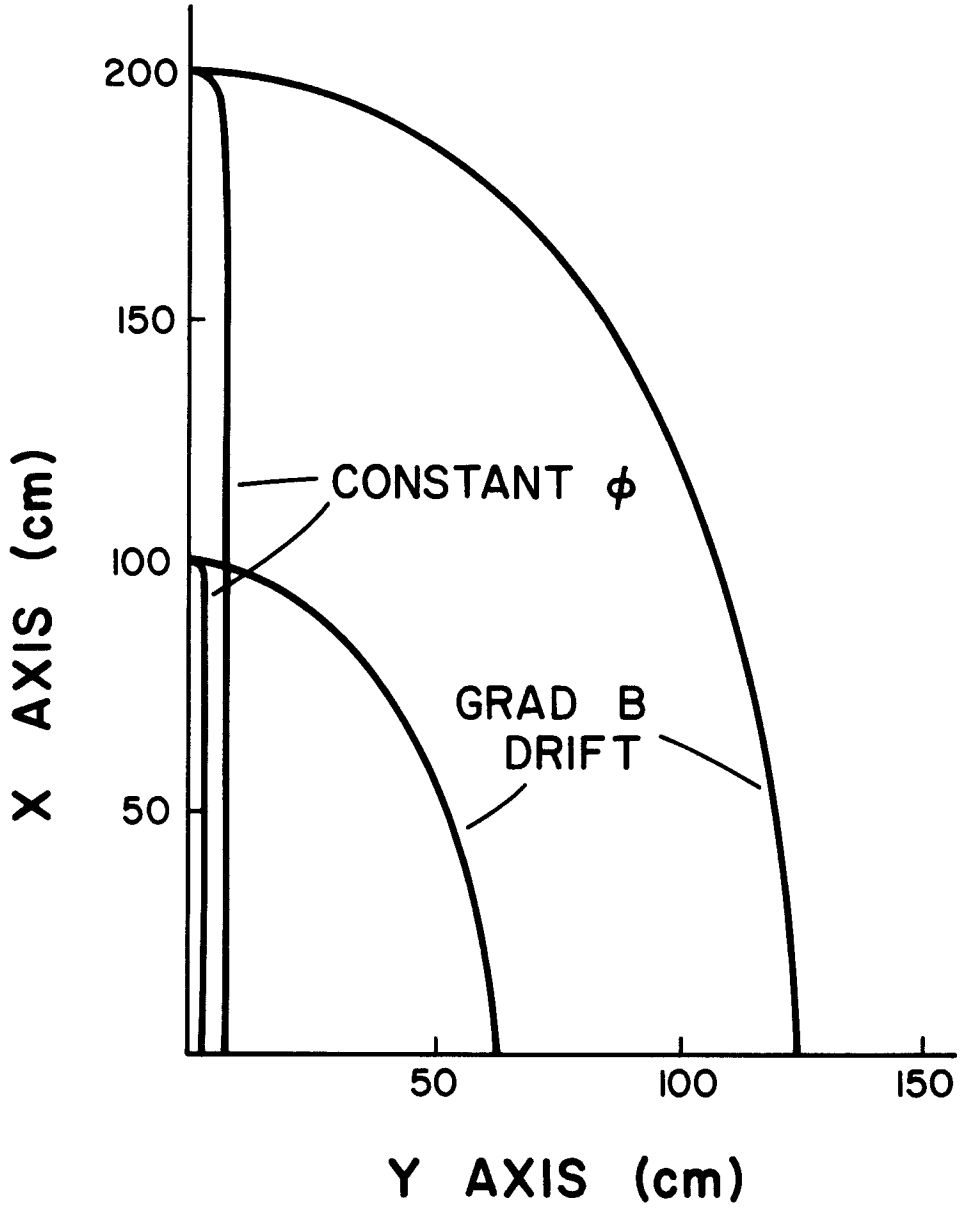

Figure 8. The $\vec{E} \times \vec{B}$ and grad-B drifts of the barrier minimum, double yin-yang configuration.

Table 1. Input Parameters

	Double Yin-Yang	WITAMIR
T_i (on-axis)	40 keV	32.5 keV
T_{ec} (on-axis)	40 keV	32.8 keV
T_{ep}	190 keV	123 keV
n_p	2.5×10^{13} cm^{-3}	2.73×10^{13} cm^{-3}
n_c (on axis)	1×10^{14} cm^{-3}	1.51×10^{14} cm^{-3}
$\phi_{plug\text{-}c.c.}$	145 keV	102 keV
R_{cc} (plasma)	100 cm	72 cm
$\phi_{c.c.\text{-}ground}$	277 keV	224 keV

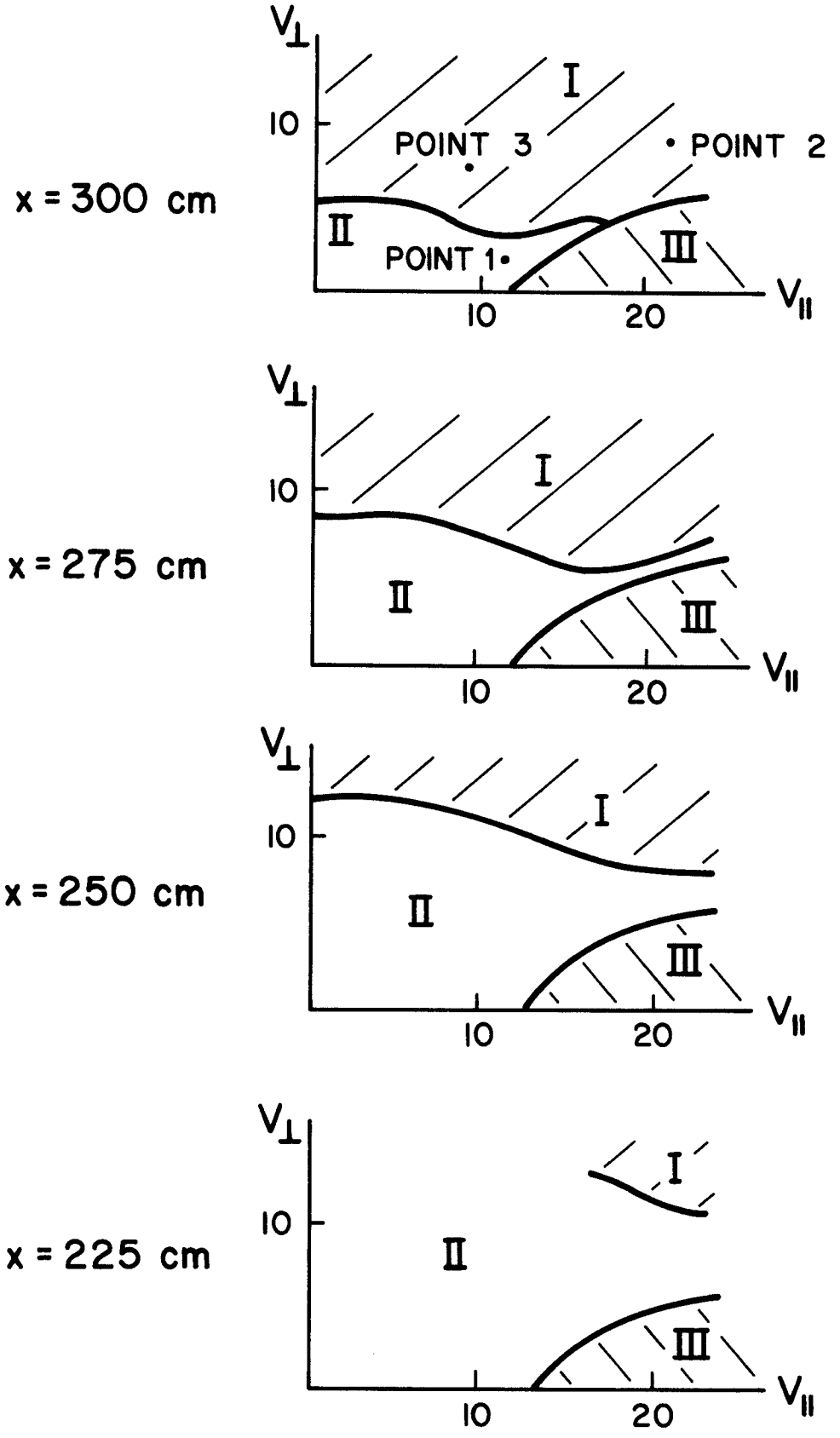

Figure 9. Ion velocity space at the barrier minimum (units of $keV^{1/2}$), double yin-yang configuration, for various points along a 367 cm major axis ellipse. Region I is the pumped region, region II is not pumped, and region III consists of passing particles.

By analyzing the surfaces of constant J the reason for this becomes apparent. This was done by comparing the value of J for a particle on the major axis, with values of J along lines making angles of 5, 10, 30, 45, 60 and 90 degrees with that axis. Values of J along these lines were computed at various radial points for the same E and μ of the on-axis particle. J was found to be monotonically increasing as one moved radially outward along these lines, and the particle's intercept could then be found from the initial value of J. (This monotonic radial dependence of J is what simplified the calculation of effective pumping in velocity space to be just a comparison of the J value at the plasma boundary.)

Figure 9 shows the location in velocity space of 3 points; the first near the loss cone, the second strongly pumped, and the third of large pitch angle. Figures 10, 11, and 12 show the drift surfaces and constant potential surfaces for these particles. Compared with the two competing drifts shown in Fig. 8, these plots show that the drift path is close to that predicted solely by the $\vec{E} \times \vec{B}$ drift. The radial potential gradient here is too large, and the resulting $\vec{E} \times \vec{B}$ drift too strong, so that it dominates the grad-B drift that would produce effective pumping.

IV. Drift Surface Analysis in the Barrier Cell of WITAMIR

The Wisconsin tandem mirror reactor design[2], WITAMIR-I, was also investigated using the techniques of the previous section. The barrier cell in this configuration is produced by a group of solenoid coils that create a 14 T peak magnetic field on axis. The minimum B end plug is created by a set of yin-yang coils. The coil arrangement is shown in Fig. 13. The flux surfaces through the barrier are therefore circular until the barrier minimum, where they grow in ellipticity going into the plug. This flux behavior is

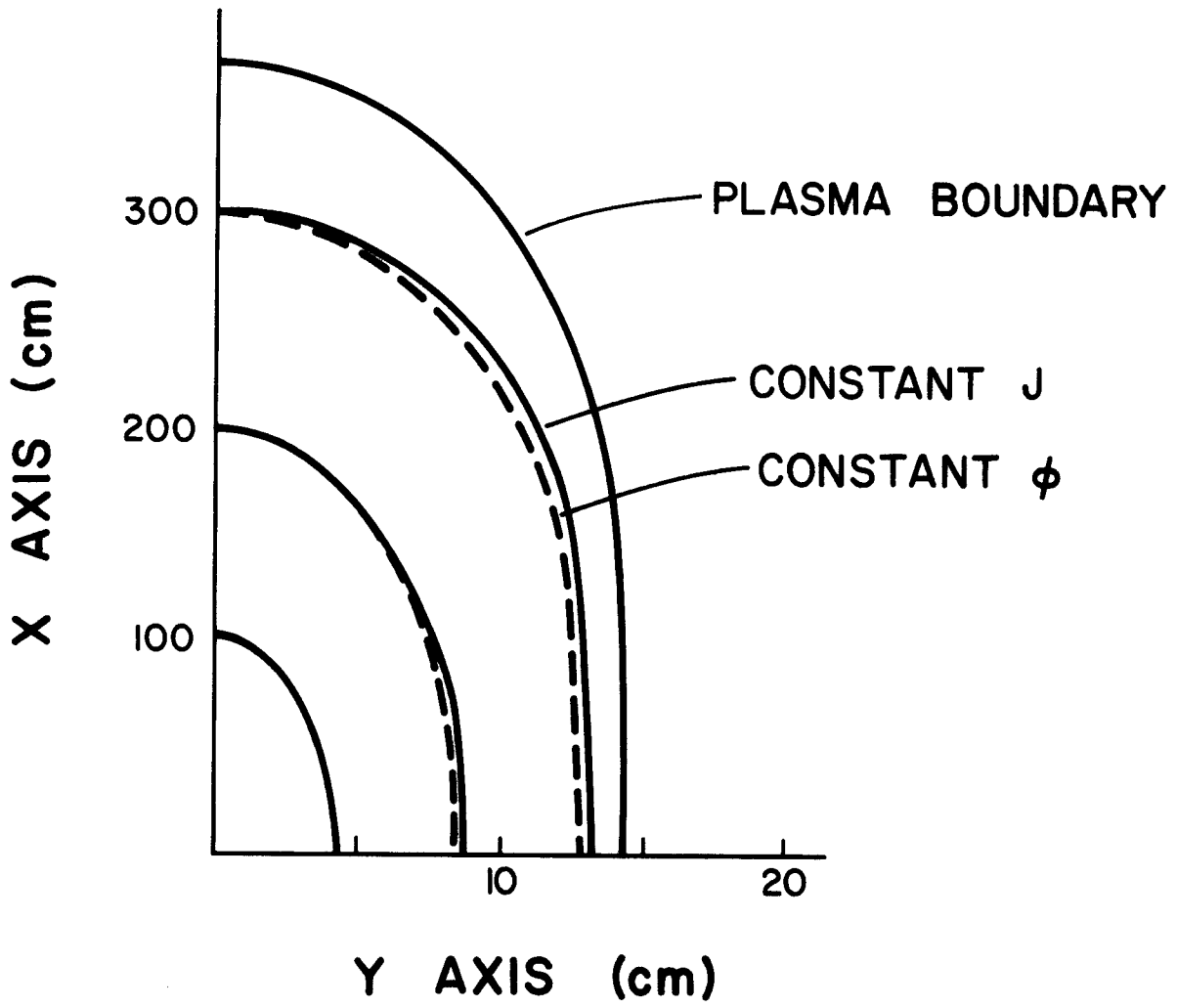

Figure 10. Surfaces of constant J and ϕ for a particle near the loss cone, point 1 of Fig. 9, at the barrier minimum, double yin-yang configuration.

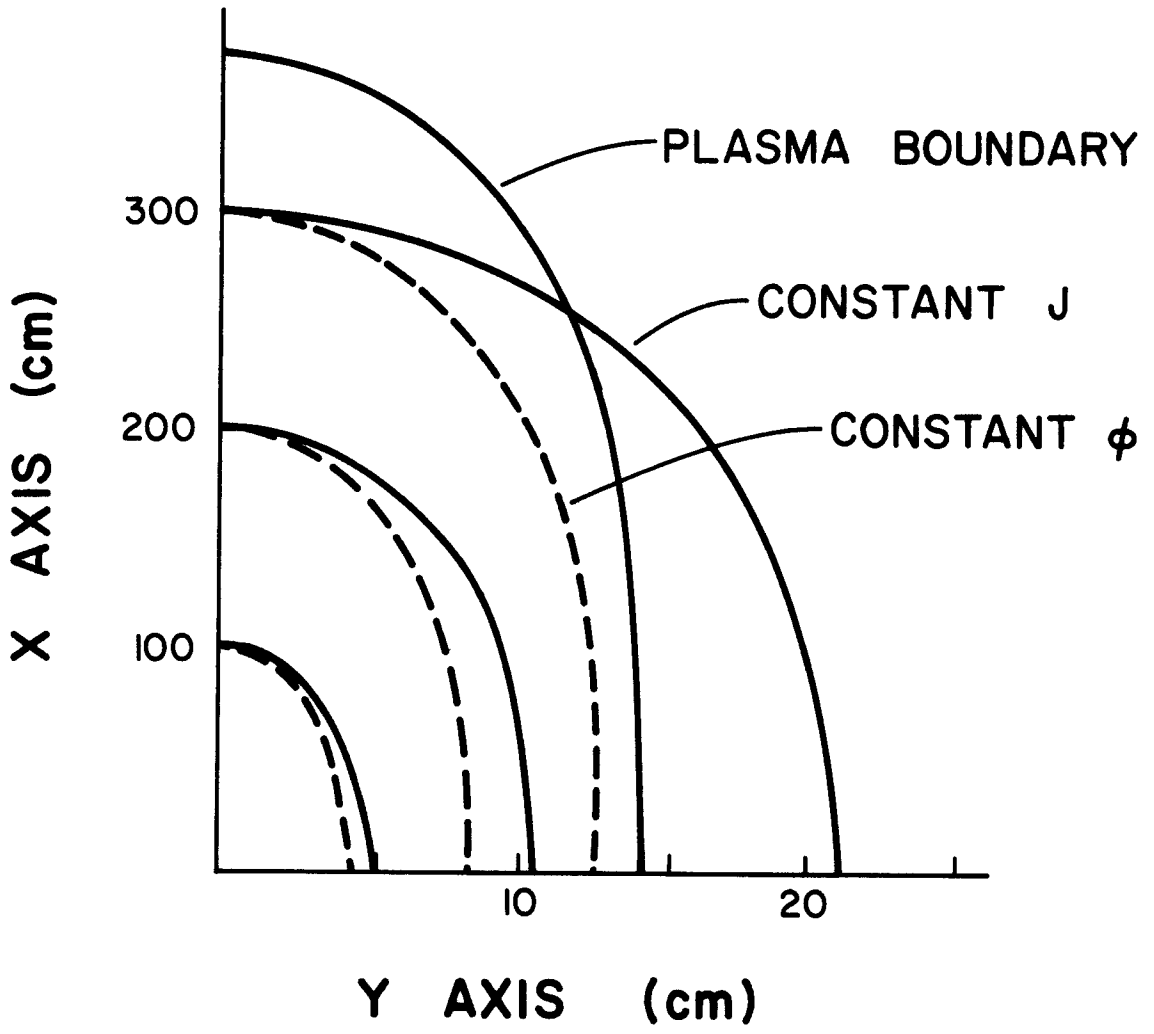

Figure 11. Surfaces of constant J and ϕ for a strongly pumped particle, point 2 of Fig. 9, of the barrier minimum, double yin-yang configuration.

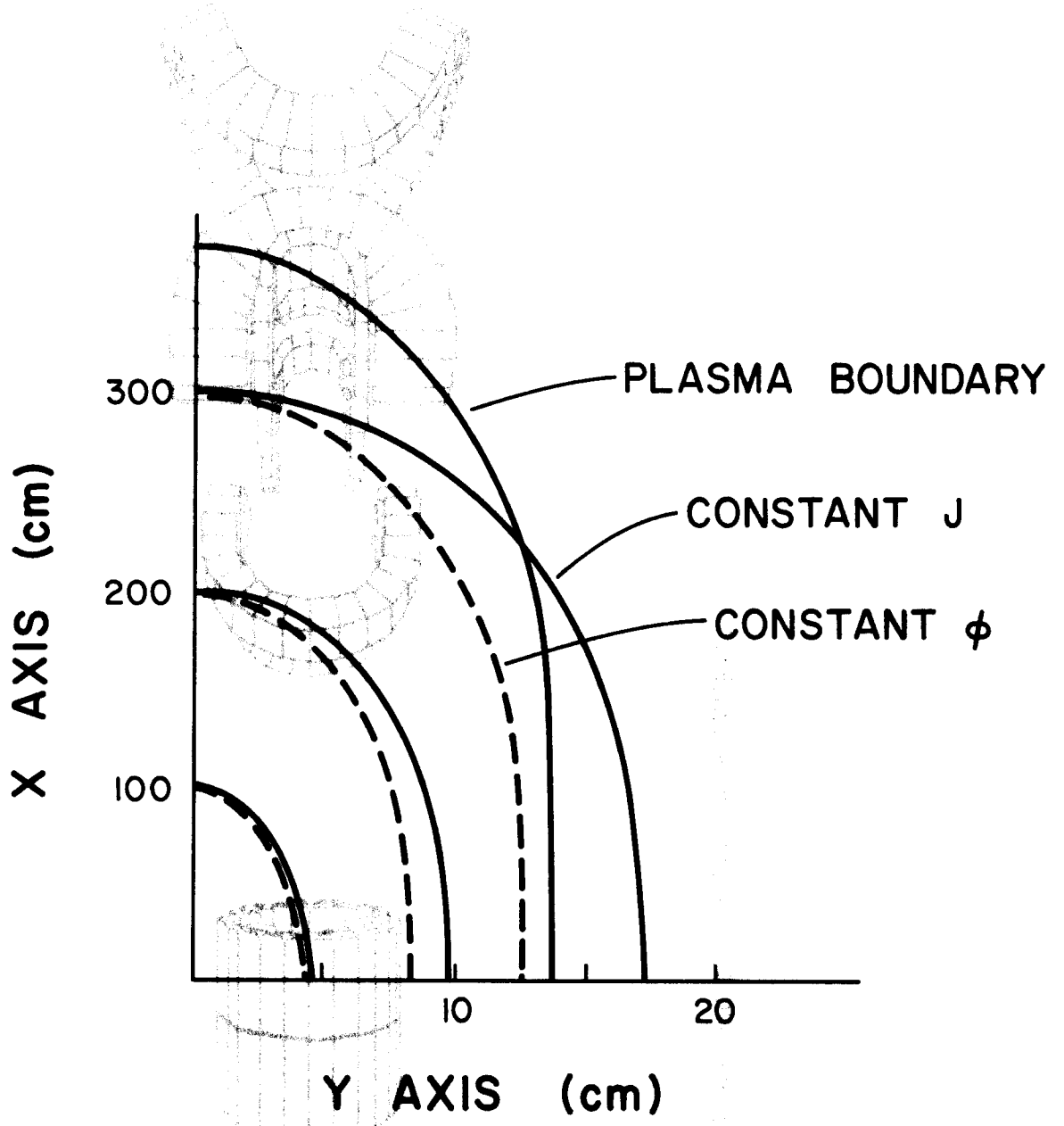

Figure 12. Surfaces of constant J and ϕ for a large pitch angle particle, point 3 of Fig. 9, at the barrier minimum, double yin-yang configuration.

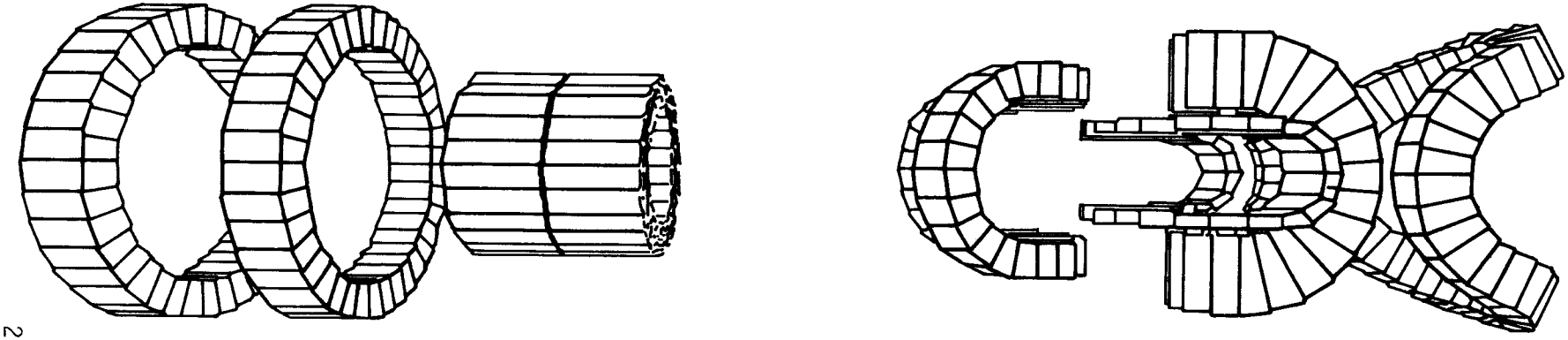

Figure 13. Barrier cell and end plug coils for WITAMIR-I.

shown in Fig. 14, along with the on-axis magnetic field and potential calculated from Eqs. (7). The potential in the plug was calculated by knowing the design maximum, ϕ_D, and then scaling with the plug mirror ratio so that the resulting potential is continuous. The input parameters used in the WITAMIR analysis are in Table 1.

Since this configuration is to a large extent axisymmetric, one does not expect to see the non-axisymmetric features of Section II. It was found that there is little variation of potential in the flux surfaces, that is, the surfaces of constant ϕ are very nearly the same as the flux surfaces, in contrast to the double yin-yang configuration. This is illustrated in Fig. 15. Also, the deviation of the drift surfaces from constant ϕ surfaces is small. Figures 16 and 17 show these surfaces at the barrier minimum for two trapped particles in velocity space near the streaming ion loss cone, and Fig. 18 shows them for a high pitch angle particle. Figure 19 shows the location of these points in velocity space. Whereas the constant ϕ surfaces are very nearly circular, the constant J drift surfaces are slightly elliptical along the x-axis, which is the major axis of the flux surfaces' ellipses in the end plug. The ellipticity there is approximately 24, so the small variation of the drift surfaces from constant ϕ surfaces again shows the dominance of the $\vec{E} \times \vec{B}$ drift over grad-B effects, as in the double yin-yang configuration. Figures 16, 17, and 18 also show that the variation of the drift surfaces is smallest for the high pitch angle particle, as one would expect since it is strongly trapped and doesn't experience the grad-B effects that lower pitch angle particles do, since they penetrate further into the plug.

From the above analysis of the drift orbits, one would expect drift-orbit pumping to be restricted to a small number of particles within a few

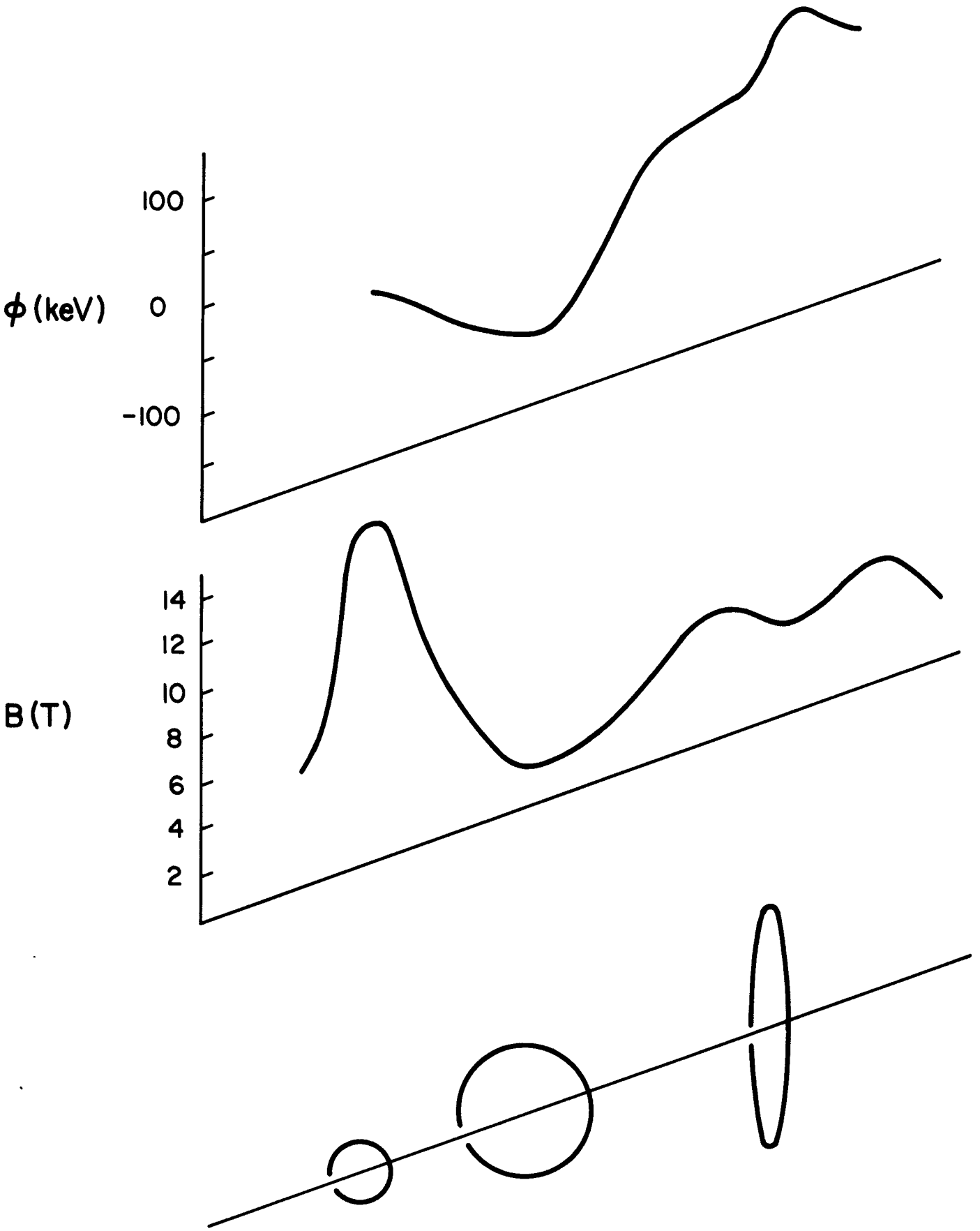

Figure 14. Flux tube through the barrier cell of WITAMIR-I, and on-axis magnetic field and potential.

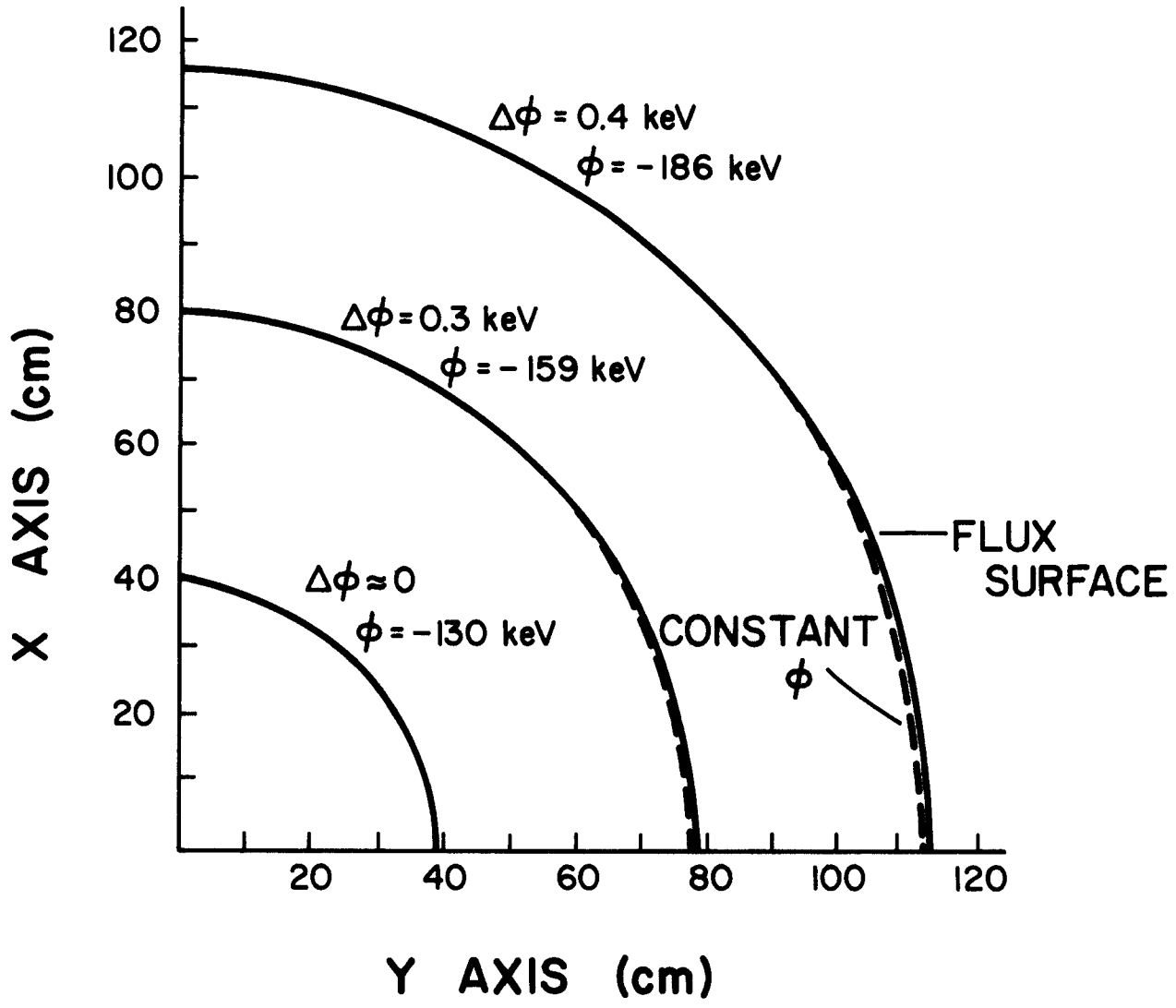

Figure 15. Variation of the potential in flux surfaces at the barrier minimum of WITAMIR-I.

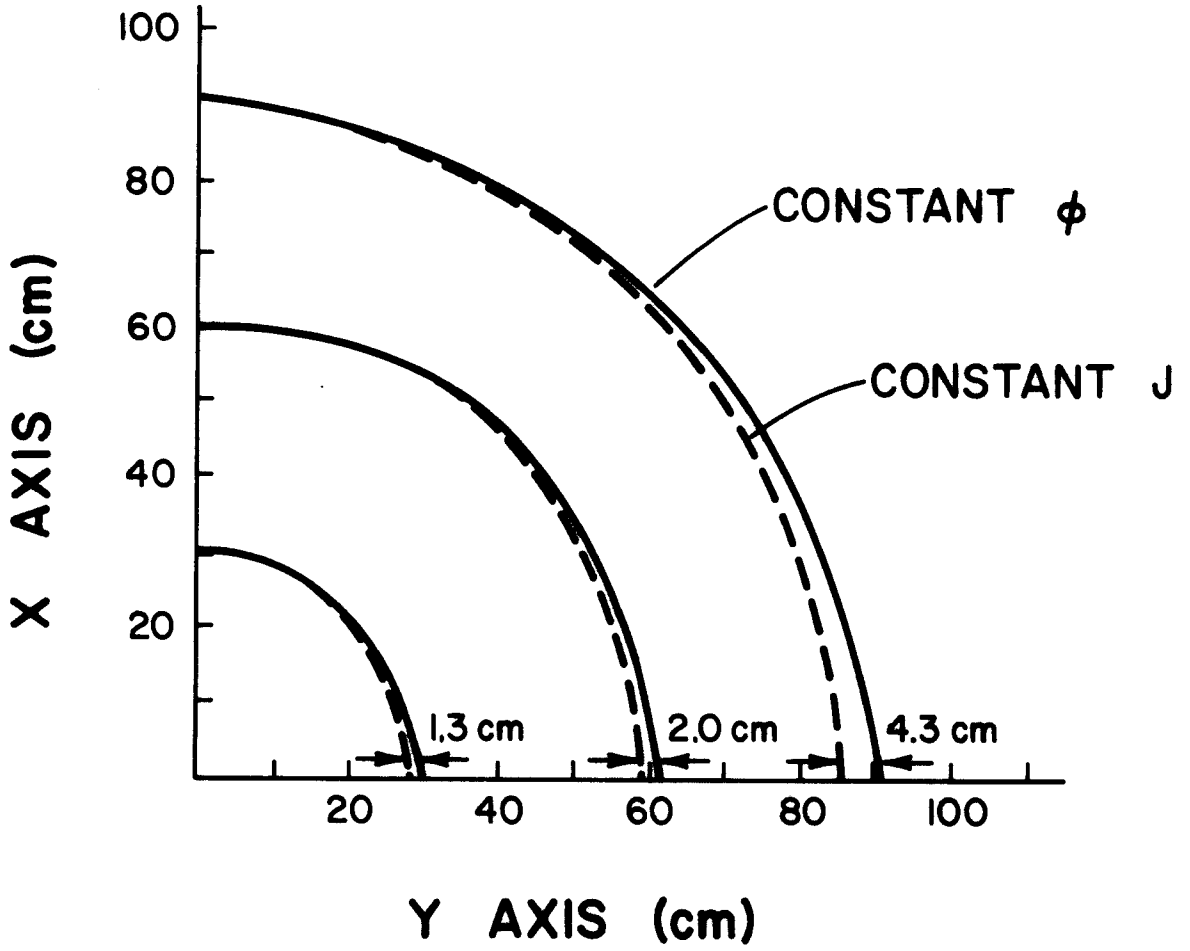

Figure 16. Surfaces of constant J and ϕ for a particle near the loss cone, point 1 of Fig. 19, at the barrier minimum of WITAMIR-I.

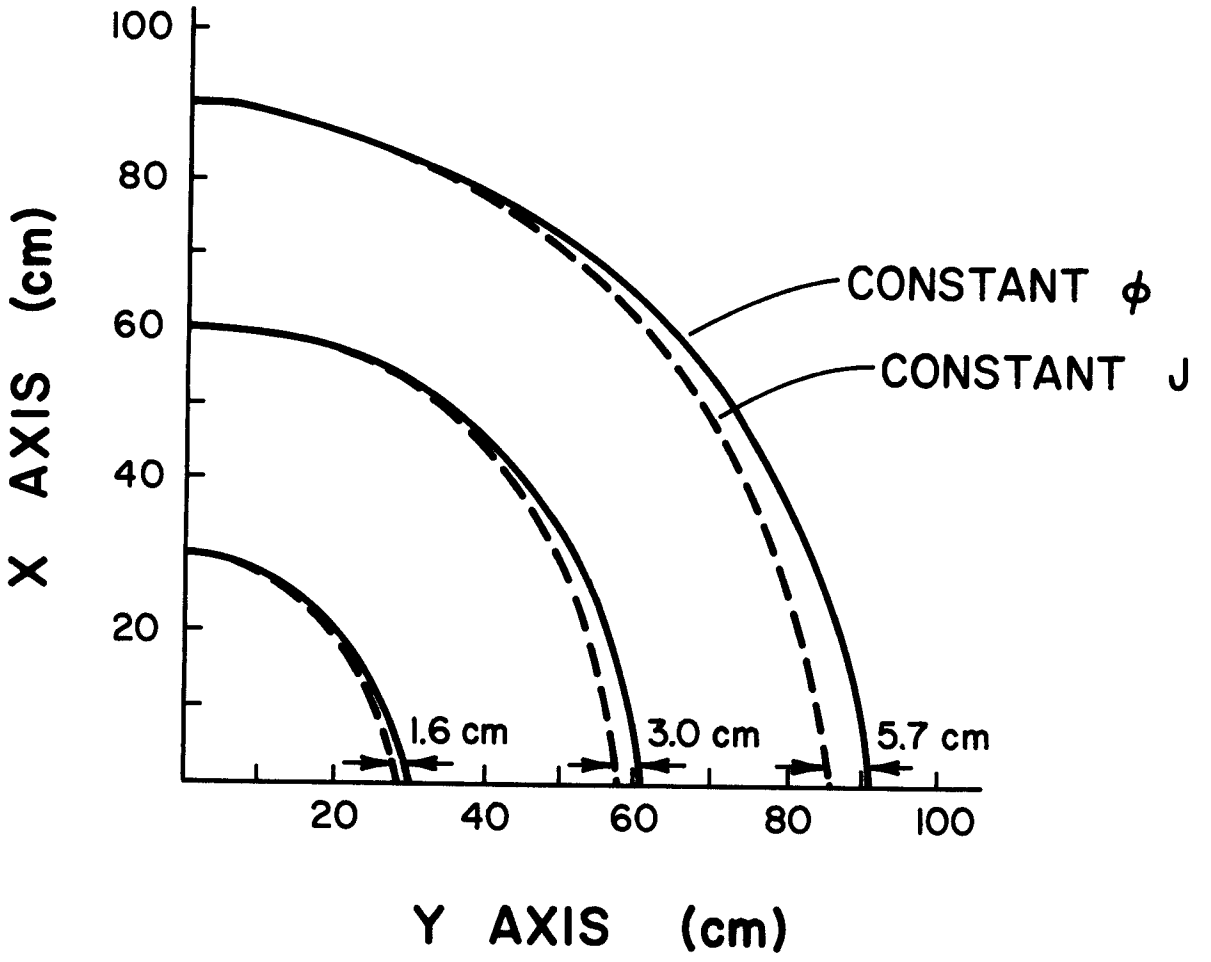

Figure 17. Surfaces of constant J and ϕ for a particle near the loss cone, point 2 of Fig. 19, at the barrier minimum of WITAMIR-I.

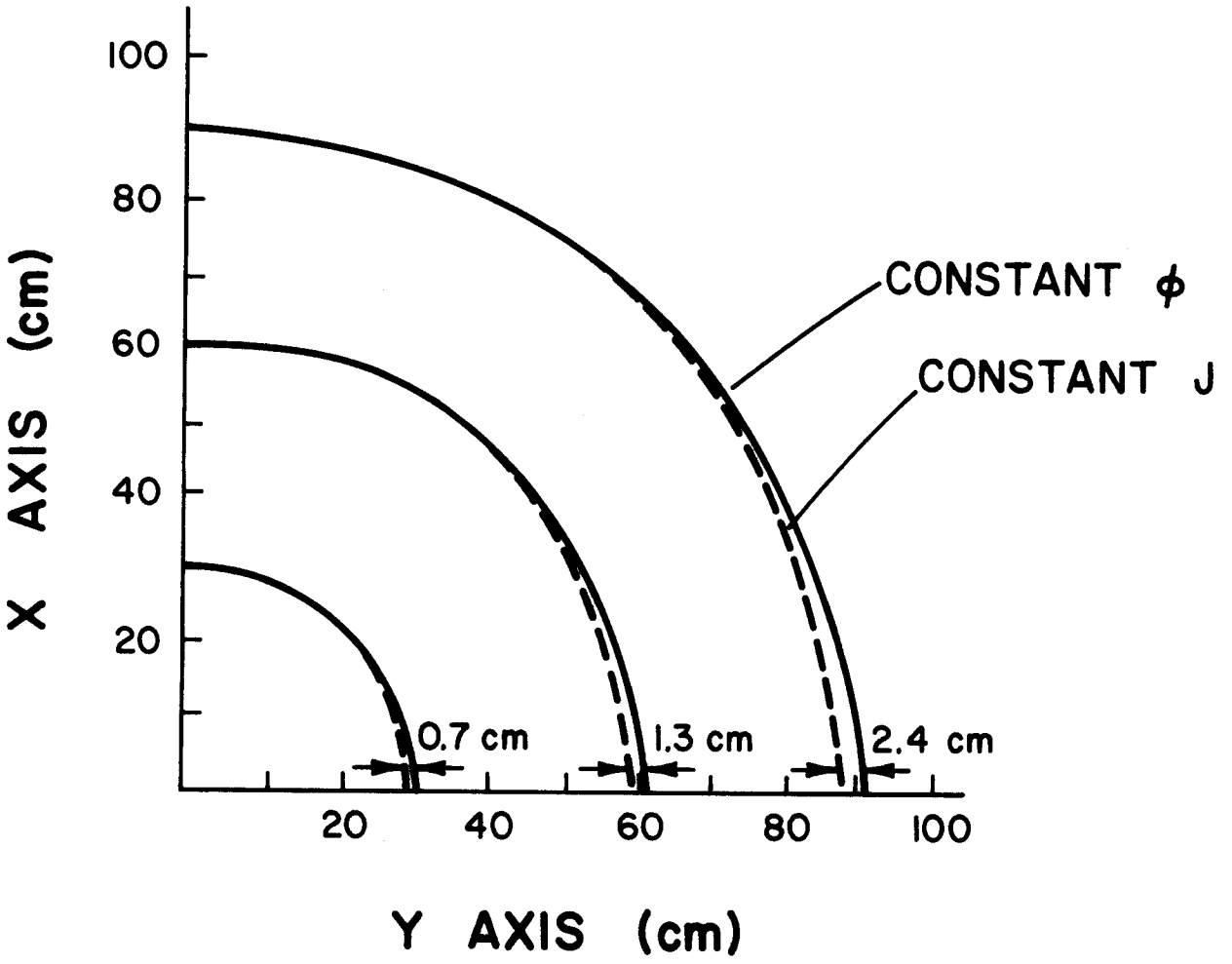

Figure 18. Surfaces of constant J and ϕ for a high pitch angle particle, point 3 of Fig. 19, at the barrier minimum of WITAMIR-I.

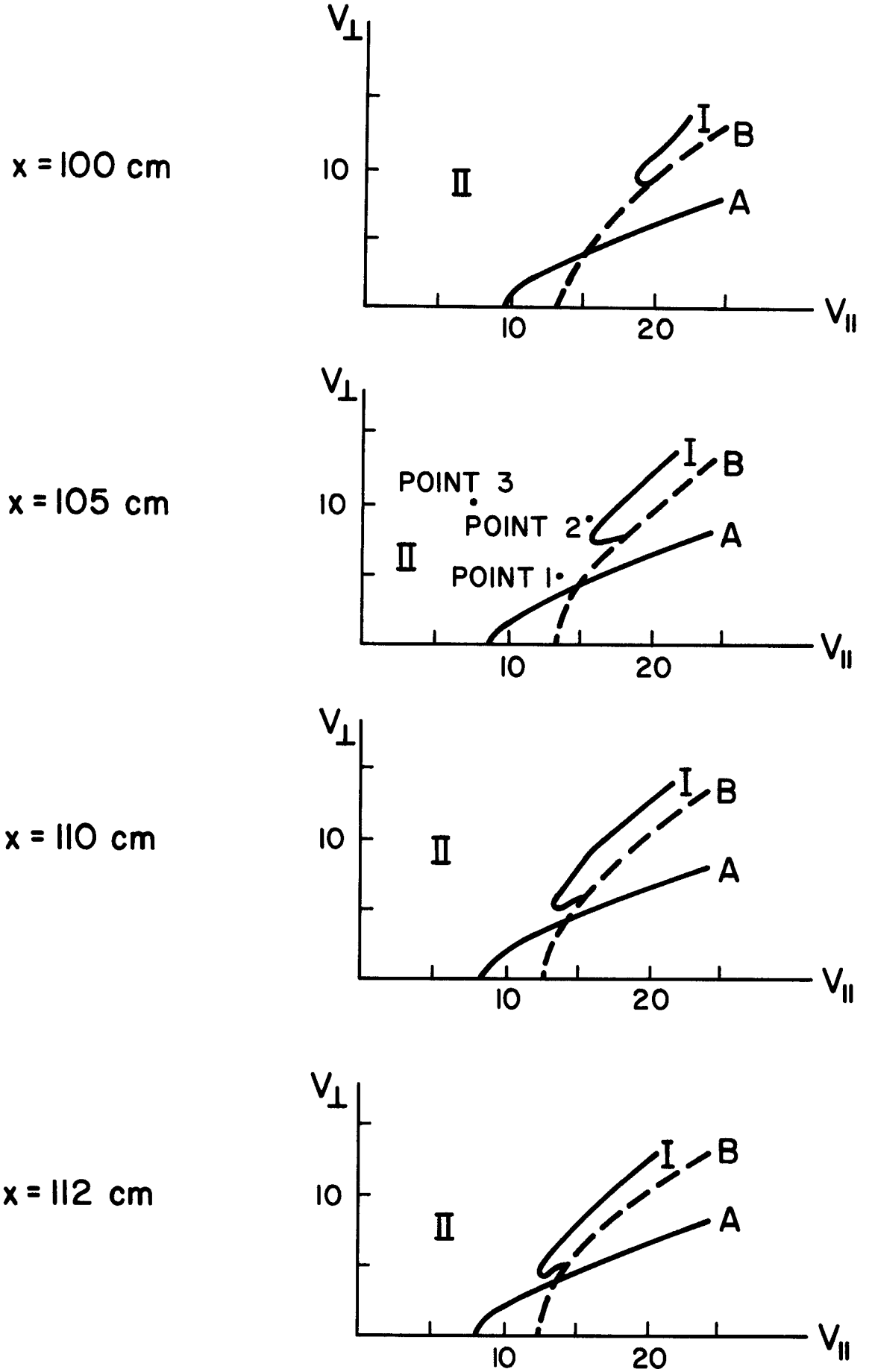

Figure 19. Ion velocity space at the barrier minimum of WITAMIR-I (units of $keV^{1/2}$) for various points along the x axis of a nearly circular plasma, boundary at x = 113.6 cm. Region I is the pumped particles, lines A and B represent the central cell and plug loss cones.

centimeters of the plasma's y-axis boundary (at y = 115.3 cm), whose elliptical drift-orbits take them out beyond the x-axis boundary (at x = 113.6 cm). In fact, although pumping is possible and only for a small class of particles, it is in the opposite sense, i.e. ions near the x-axis boundary drift out beyond the y-axis plasma boundary. That these drifts are different from those previously analyzed further inside the plasma is because the magnetic field in the fans of the plug ellipse is significantly lower (~ 40%) than it is near the axis. This means that trapped particles on field lines that go into these fans, i.e. field lines near the x-axis plasma boundary, are not magnetically reflected as strongly as they would be on y-axis field lines that map into the plug ellipse's minor axis. Thus, the integration of $v_{\parallel}$ yields larger values of J along these lines into the fans, which predicts a particle will be outside of the plasma after a 90° azimuthal drift. This tendency is weakened by the electrostatic potential, whose contribution to particle reflection does not vary strongly azimuthally. Therefore, this effect is limited in position space to those regions near the plasma edge, and limited in velocity space to particles near the plug loss cone which travel far enough into the plug to sample the variation in magnetic field.

The ion velocity space at the barrier minimum is shown in Fig. 19. Line A is the central cell loss cone and line B represents the plug loss cone so that below them would be streaming ions. Particles in Region II are barrier trapped and those in Region I are those that would be pumped. Units are again $keV^{1/2}$. Figure 19 shows velocity space for four x-axis points, all within 12% of the plasma boundary at x = 113.6 cm. It is seen that this pumping effect does border on the plug loss cone, and disappears as one moves into the plasma

as the azimuthal magnetic field variation becomes smaller and the required radial drift for pumping becomes larger.

Summary

An analysis of drift surfaces and the possibility of drift-orbit pumping has been done by calculating numerically the surfaces of constant J. In this evaluation an electrostatic potential model has been used that includes the potential's variation along a field line as a function of magnetic field, and also the radial variation of the potential. The drift surfaces obtained have been dominated by the $\vec{E} \times \vec{B}$ drift. Even in a configuration designed to maximize the grad-B drift away from the flux surfaces, the radial electric field was too strong to allow significant particle excursions. Thus, pumping by drift orbits was only effective for a portion of the trapped plasma.

In WITAMIR-I, an axisymmetric barrier configuration, the constant potential surfaces are very nearly the same as the flux surfaces, and the drift surfaces deviate slightly from these. There is, however, in this configuration a small zone of pumping caused by the non-axisymmetric plug.

Acknowledgments

The authors gratefully acknowledge helpful discussions with Prof. J. D. Callen, Dr. J. Kesner, Dr. J. Santarius, Dr. J. M. Gilmore and Dr. X-Z. Li. This research was supported by DOE.

References

1. D. E. Baldwin and B. G. Logan, Phys. Rev. Lett. 43, 1318 (1979).

2. B. Badger et al., "WITAMIR-I, A Tandem Mirror Reactor Study," University of Wisconsin Fusion Engineering Program Report UWFDM-400 (1980).

3. J. Kesner, Comments of Plasma Physics and Controlled Fusion, 5, 123 (1979).

4. D. E. Baldwin, B. G. Logan, T. C. Simonen, eds., "Physics Basis for MFTF-B," Lawrence Livermore Laboratory Report UCID-18496 (1980).

5. J. M. Gilmore, "Plasma Buildup in Tandem Mirror Machines," Ph.D. Thesis, Univ. of Wisconsin (1980).

6. J. Kesner, "Barrier Cell Sheath Formation," University of Wisconsin Fusion Engineering Program Report UWFDM-348 (1980).

7. X-Z. Li and G. A. Emmert, "The Electrostatic Potential Profile in a Tandem Mirror Thermal Barrier," University of Wisconsin Fusion Engineering Program Report UWFDM-392 (1980).